All-fiber phase shifter based on hollow fiber interferometer integrated with Au nanorods

Meng Luo[a], Xinghua Yang[a,*], Pingping Teng[a], Zhihai Liu[a], Depeng Kong[b], Jianzhong Zhang[a], Jun Yang[a], Fengjun Tian[a], Danheng Gao[a], Zhanao Li[a], Libo Yuan[a,c], Kang Li[d], Nigel Copner[d]

[a]*Key Lab of In-Fiber Integrated Optics, College of Physics and Optoelectronic Engineering, Harbin Engineering University, Harbin 150001, China*

[b]*State Key Lab of Transient Optics and Photonics, Xi'an Institute of Optics and Precision Mechanic, Chinese Academy of Sciences, Xi'an 710119, China*

[c]*Photonics Research Center, Guilin University of Electronics Technology, Guilin 541004, China*

[d] *Wireless & Optoelectronics Research & Innovation Centre, Faculty of Computing, Engineering & Science, University of South Wales, Wales, CF37 1DL, UK.*

*Corresponding author: yangxh@hrbeu.edu.cn

Keywords: In-fiber devices; All-fiber integrated devices; Au nanorods; Phase shifter

ABSTRACT

We propose and demonstrate a novel all-fiber phase shifter by integrating a microstructured hollow fiber (MHF) and gold nanorods (GNRs) with photothermal effect. There are two cores and a central hole in the MHF. One core is suspended on the inner surface of the central hole, which serves as the sensing arm. The other one located in the cladding is as the reference arm. A Mach-Zehnder interferometer (MZI) can be fabricated simply through splicing multimode fiber-single mode fiber structures at both ends of the MHF. In this device, the center hole of MHF is filled with the solution of GNRs. The GNRs around the sensing arm is excited by near infrared light in the core via the evanescent interaction and the released heat because of the photothermal effect. Then, the refractive index around the sensing arm is modulated and the interference dips can be reversibly shifted. Experimental results show that a spectral shift efficiency of -37.5 pm/mW at the wavelength of 1550 nm can be obtained under an excitation laser at the wavelength of 805 nm. This all-optical device based on MHF and GNRs has great potentials in integrated all-fiber signal controlling.

1. Introduction

Optical phase shifters have attracted the increasing attention of researchers, and they are mostly fabricated through optical path variation schemes [1-4]. Compared with traditional mechanical deformation and acoustic photoelectric technology, all optical phase shifters have the advantages of higher control accuracy, low cost and strong robustness [5]. At present, they have been widely used in many fields such as optical communication, interference sensors, optical interference systems and signal processing. Among them, optical fibers can be easily fabricated to produce an all-fiber phase modulator. The all-fiber phase shifters made of optical fiber have directly used in integrated electro-optical systems, fiber lasers, wavelength division multiplexing (WDM) fiber-optic communication systems, and fiber-optic sensing systems for its efficient optical coupling, low insertion loss, low back reflection, and compact package [6-8]. Up to now, optical fiber phase shifters had been achieved mainly by cross-phase shift modulation, stimulated Brillouin scattering and Brillouin scattering [9-12]. In particular, a viable method such as doping transition metal, color centers, or rare earths in the fiber has been proposed. On account of weak intrinsic non-linearity in silicate, therefore, it often requires intensity pumping light and fiber lengths of up to several kilometers for optical modulation.

On the other hand, varieties of nanoparticles have been applied in many fields, such as imaging, diagnosis, and therapy due to the strong photothermal effect [13-15]. Among them, as a kind of photothermal conversion materials in nanoscale, GNRs show efficient electric dipole absorption to the NIR light in the 800 to 1000 nm spectral range and present an efficient photothermal effect. The local heating by the resonant excitation of surface plasmon polaritons (SPP) in metal-dielectric nano-composites of GNRs can be obtained [16, 17].

In this paper, we experimentally realized a compact and efficient all-optical phase shifter. It was based on an optical fiber Mach-Zehnder interferometer (MZI) fabricated from a microstructured hollow fiber (MHF) and the photothermal effects of trace amount of gold nanorods (GNRs). The internal hole of MHF was filled with GNRs and the GNRs were excited by the NIR light at 805 nm by the evanescent field of the suspended core. A subsequent optothermal process of the GNRs varied the RI around the suspended core, and caused the change of the optical path difference of the two arms. Then, the photothermal effect directly determined the displacement of the output spectrum.

2. Experiment setup of the all-fiber phase shifter

The optical path of the proposed phase shifter is illustrated in Fig. 1. The signal light was from an amplified spontaneous emission (ASE) light source from 1520 to 1620 nm. The pump light was a laser diode with the center wavelength of 805 nm and it was used to control the phase shift of the fiber interferometer. A WDM coupler was used to combine the signal and control lights and allowed them to

be injected into the MZI. This specially designed and fabricated MHF by us has a tubular cladding, a suspended core, a central air hole and a core in the cladding. The cross section of a MHF is shown in the inset of Fig. 1. The diameter of the two cores was 8 μm. The outer diameter of the fiber was 125 μm in accordance with the SMF. In this device, both ends of the MHF were spliced with a piece of multimode fiber (MMF, core/cladding diameters of 105/125 μm) with the length of 1 mm and then spliced with SMF, respectively. Then, the MMF could couple SMF light into the two cores of the MHF and integrate the light in the two optical paths together to generate interference. Specifically, when splicing the left end of the MHF with the MMF, a laser with the wavelength of 650 nm was coupled into the light path and optical output field of MHF was observed by a CCD camera. At the same time, by adjusting the relative position between the MMF and the HTCF in the fusion splicer, an interference pattern of the MHF exit light field is obtained and the two ends can be spliced together. Similarly, at the second spliced point between MMF and the right end of the MHF, the OSA is used to monitor the output interference spectrum during adjusting the offset distance between the MMF and the MHF. When the obvious interference spectrum was observed by OSA, the two ends were spliced together. The main parameters of the fusion splicer (JiLong, KL-260B) is set as the pre-splicing time of 50 ms, the splicing current of 13 mA, and the splicing time of 0.3 s. By discharging four times, the MMF and MHF can be spliced together. The fabrication process of the MZI integrated with GNRs was shown in Fig. 1(b).

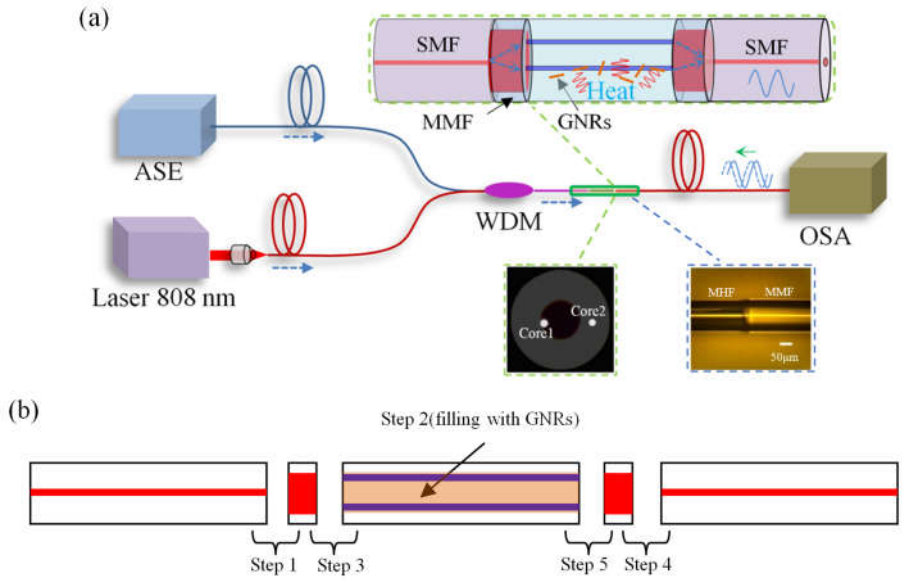

Fig. 1. (a) Schematic diagram of all-fiber phase shifter based on MZI integrated with the GNR solution. Inset: cross section of the MHF and the spliced region between MMF and MHF. (b) Sketch of the fabrication process of the MZI integrated with GNRs.

3. Characterization of the evanescent field of the MHF and the in-fiber MZI

To confirm the evanescent field of the suspended core of the MHF, a fluorescein ($C_{20}H_{12}O_5$) solution with RI of 1.4350 was injected into the device. The $C_{20}H_{12}O_5$ could produce 490-570 nm fluorescence signals in the 400-450 nm spectrums. The light with the wavelength of 450 nm was coupled into the suspended core through the WDM, and the solution around the core was observed under a fluorescence microscope. Fig. 2 shows the experiment results. The micrograph of the device without stimulation with the light source was shown in Fig. 2(a). In the case of the light source turning on, the $C_{20}H_{12}O_5$ inside the central hole was excited by the evanescent field of the suspended core to emit intensive green fluorescence. This result was showed in Fig. 2(b).

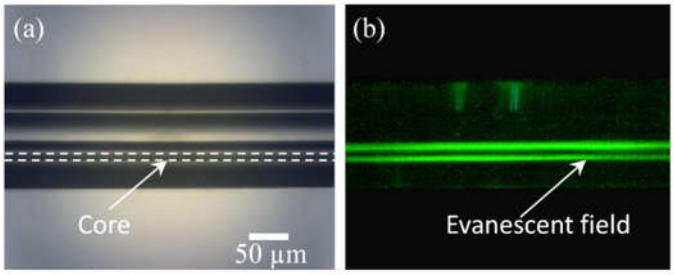

Fig.2. (a) Side-view of the MHF under a microscope. (b) Characterization of the evanescent field of the suspended core in the MHF.

The RI sensitivity of the MZI was investigated. Here, another MZI (the length of MHF is 15 cm) with opening holes at both ends of the MHF was built. Different solutions were alternately injected into the center hole. The result was summarized in Fig. 3. It is clearly observed that the interference spectrum shifted obviously with the change of the RI from 1.3313 to 1.3345. From the inset, when the RI only changed 0.0011, the corresponding shift of the spectra was about 2.76 nm. The wavelength showed a linear relationship with the change of RI. From the fitting line, this device performed the sensitivity of about 2490 nm/RIU.

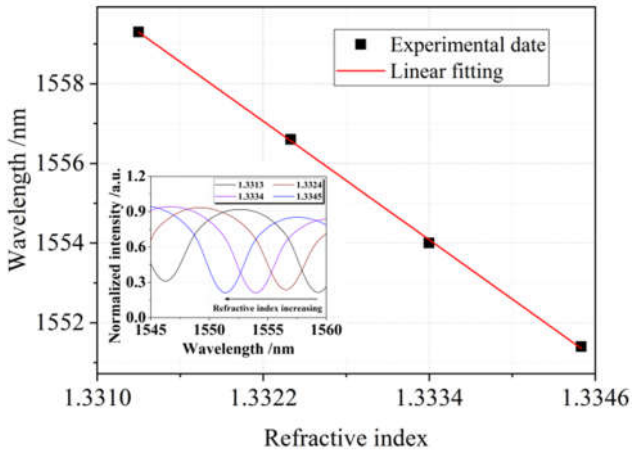

Fig. 3. RI sensitivity of the device. Inset: spectrum shift of the interference with the change of RI

To investigate the thermal response of the interferometer, the device was placed in a thermostatic drying oven. The temperature was gradually increased from 40°C to 80 °C. As a result, the transmission spectrum exhibited shift which was observed. We can observe that the temperature and phase shift show good linearity, and the linear regression equation could be expressed as y=-40x+1547.66. The temperature sensitivity is about -40 pm/° C. The expert results were shown in Fig. 4. This temperature-induced phase shift is due to the change of the optical path difference in this fiber interferometer. When the MZI was filled with the solutions containing GNRs, the temperature can be adjusted by the photothermal effect of the GNRs which is stimulated by the evanescent field of the suspended core. Then, the RI around the core and the optical path difference between the two cores in the MZI can be changed. Finally, the interference spectrum of the device can be shifted.

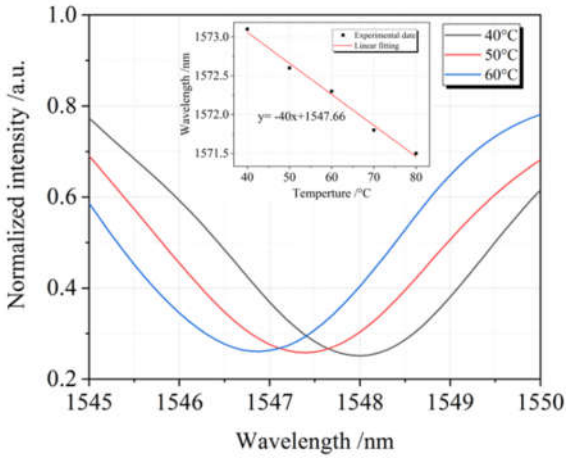

Fig. 4. Temperature sensitivity of the device. Inset: linear fitting of the interference with the change of temperature

4. Phase shift principle of the interference spectrum of the MZI

When the incident light beam traveling in the fiber core of MMF arrived at the welding region of MHF, it was divided into two parts: one was coupled into the core in tubular cladding and the other was coupled into the suspended core. At the other end of the MHF, the beam recombined to produce an interference pattern in SMF. The interfering light intensity could be explained as follows [18, 19]:

$$I_T = I_c + I_s + 2\sqrt{I_c I_s}\cos(\Delta\varphi)$$

where I_c and I_s represent the intensities of the light in the cladding core and the suspended core, respectively. $\Delta\varphi$ is the phase difference, and it can be defined as following:

$$\Delta\varphi = \frac{2\pi}{\lambda}\Delta_n L$$

where the wavelength of propagating light is represented by λ. Δ_n is the difference of the effective RI between two interfering cores, and it is changed by changing the effective RI of $n_{core\ 1}$ or $n_{core\ 2}$. In the proposed device, through the evanescent field of the suspended core, 805 nm light transmitted into the solution where the GNRs were located. Because of the photothermal effect of GNRs, the temperature

and the effective RI of the liquid around the core 2 can be changed, so the optical path difference of the two coherent lights changes. Then, at the output of the MZI, phase shifts could be recorded by OSA.

5. All-fiber phase shifting characteristics of the device

The absorption spectrum of GNRs (purchased from Nanjing Nanoeast Biotechnology Co., Ltd.) in the experiment was shown in Fig. 5. A broad peak at 826 nm can be observed. Then, a control light at 805 nm which was very close to the absorption peak for generating photothermal effects was coupled into the light path. In the following experiment, in order to satisfy the experiment condition of the solution refractive index, solid GNRs was obtained through centrifuging 1 ml of the GNRs aqueous solution at 3000 rpm/min. Subsequently, it was mixed with 1 ml of mixed solution of Dimethyl sulfoxide (DMSO) and N,N-Dimethylformamide (DMF). The RI of the resulting solution was 1.4350. The purpose was to further improving the evanescent field of the suspended core inside the MZI. The obtained solution was then inhaled into the central hole of the MHF and connected like Fig. 1.

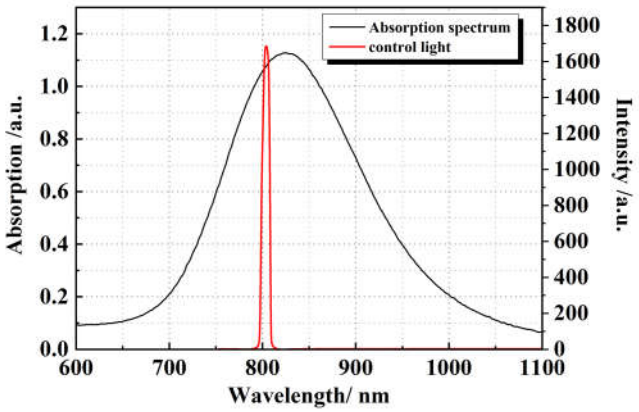

Fig. 5. Absorption spectrum of the GNRs and the control light spectrum of 805 nm.

Here, the interference spectra (the length of MHF is 40 cm) before and after GNRs filling are present in Fig. 6(a). We can observe the free spectrum range (FSR) is about 3.7 nm. Through adjusting the power of the control light at 805 nm, the output spectrum of the MZI and the phase shifts was monitored. The results were summarized in Fig. 6(b). The spectral curve when no control light was present by black. The others were shown in different colors. It can be observed that the spectrum shifts towards shorter wavelength when power of the control light increases.

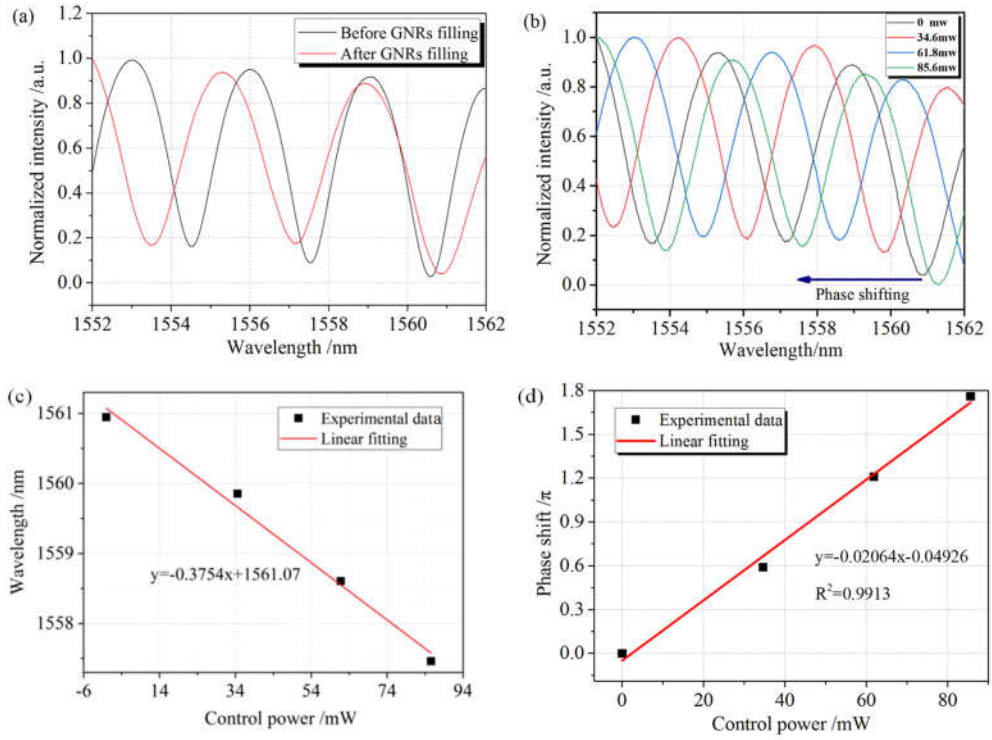

Fig. 6. (a) The interference spectra before and after GNRs filling. (b) Shifts of the interference spectral of the proposed device as a function of the control light power. (c) Linear fitting of the spectral shift as a function of the control light. (d) Linear fitting of the phase shift as a function of the control light.

As the control laser at λ=805 nm with different power were injected into the device, the spectral shifted in the same direction. In this experiment, when the power increased from 0 to 85.6 mW, the spectral shifted from 1560.82 nm to 1557.61 nm with the amount of 3.21 nm. The spectral shift efficiency is about -37.5 pm/mW. In addition, the spectral shift was linear and the liner fitting as present in Fig. 6(c). The linear regression equation could be expressed as y=-0.03754x+1561.07 with the coefficient of R^2=0.9897. The corresponding phase shift of the device is shown in Fig. 6(d). This pump power can obtain a phase shift about 1.7 π. The linear regression equation could be expressed as y=-0.02064x-0.04926 with the coefficient of R^2=0.9913. By further optimizing the structure and switching to material with higher photothermal conversion efficiency, low-pump light requirements and long-life phase modulators could be realized.

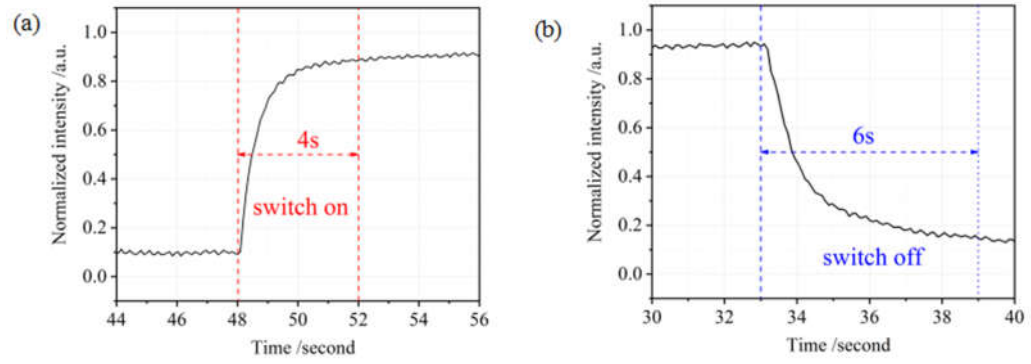

Fig. 7. Response time and recovery time at 1550 nm of the all-fiber phase shift device: (a) Response time of switching the pump light on. (b) Response time of switching the pump light off.

The dynamic characteristics of the setup were demonstrated in Fig. 7. The output light intensity of a signal light at λ =1550 nm with the power of 40 mW was monitored with switching the control light on and off. From this figure, we can observe the response time of this device when turning on and off were about 4 s and 6 s, respectively. And this hysteresis should be the time for the GNR liquid around the suspended core to warm up and cool down to reach equilibrium. Generally, this response time of the device relied on the heat transfer rate of the GNRs solution. In the case of a given heat transfer coefficient, the volume of the liquid played a decisive role. This fast rate of phase shift is because of the small volume of the solution which was about 180 nanoliters in the MHF.

The recovery and the reversibility of the all-fiber phase shifter are present in Fig. 8. The light intensity at 1550 nm was monitored when the 805 nm laser with the power of 40 mW was periodically applied. When the light was alternately turned on and off in 3 cycles within 100 seconds, the output intensity at 1550 nm presents periodic changes. Meanwhile, the response of the output power is completely reversible and reproducible. This means that the photothermal characteristics of the GNRs in the MHF remain stable after being periodically excited by the NIR light. This stable should be attributed to the in-fiber structure with GNRs which is isolate to the external influence and the reduction of the heat exchange between the inside and the outside of the MZI.

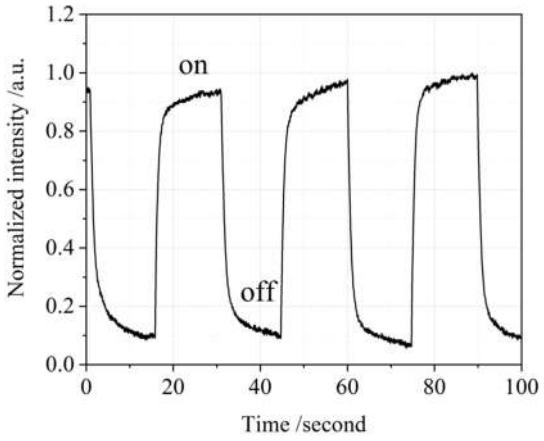

Fig. 8. Reversibility of the in-fiber phase shifter when the control light was periodically switched on and off.

To evaluate the stability of the device, the light intensity at 1550 nm was real-time monitored when the 805 nm laser with the power of 35 mW was applied. The result is shown in Fig. 9. The light intensity was tracked within 30 seconds and the intensity fluctuation was found to be approximately 5%. This fluctuation may be caused by heat exchange between the fiber optic device and the surrounding environment.

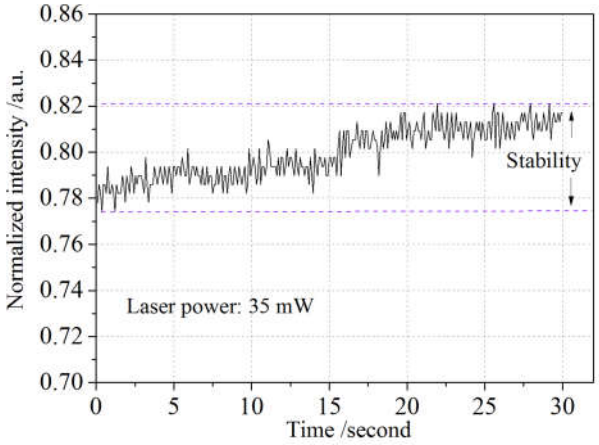

Fig. 9. Stability of the light intensity at 1550 nm when the control light was applied

6. Conclusion

In conclusion, a novel all-fiber GNR-integrated phase shifter based on an in-fiber interferometer integrated with Au nanorods was proposed. The GNRs was integrated with a specially designed MHF and incident light at 805 nm was coupled into the in-fiber interferometer, which allowed the GNRs to occur resonant photothermal effect by the evanescent field of suspended core. Then, the heat released by the GNRs was rapidly transferred to the liquid around the suspended core, and the refractive index around the core can be modulated. Finally, the incident light caused the phase shifts of the interference spectrum. Results show that when the laser at 805 nm is coupled into the light path, a phase shift of 3.21 nm at 1550 nm with the shift efficiency about -37.5 pm/mW can be obtained. The device showed repeatable and reversible optical properties. Through reducing the loss between the wedding or changing higher photothermal conversion efficiency material, the power of the pump light will be reduced. These results indicate that the developed in-fiber phase shifter has great potential applications in on-line optical devices.

Acknowledgement

This work is supported by the National Key R&D Program of China (2018YFC1503703); National Natural Science Foundation of China (NSFC, 11574061, 61405043); the Natural Science Foundation of Heilongjiang Province (LC2018026, F201405); the Fundamental Research Funds for the Central Universities(3072019CF2502).

Reference:

1. J. Yao, D. Yu, E. Li, J. Xi, and J. Chicharo, Optical phase shifting with acousto-optic devices, Opt. Lett. 30 (2005) 189-191.
2. L. Lucchetti, K. Kushnir, and A. Zaltronl, Light controlled phase shifter for optofluidics, Opt. Lett. 41 (2016)333-335.

3. A. V. Zvyagin and D. D. Sampson, Achromatic optical phase shifter–modulator, Opt. Lett. 26, (2001) 187-189.
4. J. Zhang, X. Qiao, H. Yang, R. Wang, Q. Rong, K. Lim, and H. Ahmad, All-fiber magnetic field sensor based on tapered thin-core fiber and magnetic fluid, Appl. Opt. 56 (2017)200-204.
5. K. Wu, C.S. Guo, H. Wang, X.Y. Zhang, J. Wang, and J.P. Chen, All-optical phase shifter and switch near 1550 nm using tungsten disulfide (WS_2) deposited tapered fiber, Opt. Express 25, (2017) 17639-17649.
6. T. Y. Kim, C. S. Park, M. Hanawa, and S. J. Kim, Optical delay interferometer based on phase shifted fiber Bragg grating with optically controllable phase shifter, Opt. Express 14 (2006) 4250-4255.
7. A. Bhatti, H. S. Al-Raweshidy, and G. Murtaza, Optical response of an all-fibre acoustooptic phase modulator using aluminium nitride coating, Opt. Commun. 176 (2000) 355-363.
8. O. Tarasenko and W. Margulis, Electro-optical fiber modulation in a Sagnac interferometer, Opt. Lett. 32 (2007) 1356-1358.
9. A. Loayssa and F. J. Lahoz, Broad-Band RF Photonic Phase Shifter Based on Stimulated Brillouin Scattering and Single-Sideband Modulation, IEEE Photon. Technol. Lett. 18 (2005) 208-210.
10. W. Liu and J. Yao, Ultra-wideband microwave photonic phase shifter with a 360° tunable phase shift based on an erbium-ytterbium co-doped linearly chirped FBG, Opt. Lett. 39 (2014) 922-924.
11. H. Shahoei and J. Yao, Continuously Tunable Slow and Fast Light by Using an Optically Pumped Tilted Fiber Bragg Grating Written in an Erbium/Ytterbium Co-Doped Fiber, IEEE Photon. Technol. Lett. 24 (2012) 818-820.
12. K. Qian, L. Zhan, H. Li, X. Hu, J Peng, L. Zhang and Y Xia, Tunable delay slow-light in an active fiber Bragg grating, Opt. Express. 17 (2009) 22217-22222.
13. R. Lv, C Zhong, R Li, F He, Z Hou, S. Gai, C. Li, and P. Yang, Multifunctional Anticancer Platform for Multimodal Imaging and Visible Light Driven Photodynamic/Photothermal Therapy, Chem. Mater. 27 (2015) 1751-1763.
14. S. Gai, C. Li, P. Yang and J Lin, Recent Progress in Rare Earth Micro/Nanocrystals: Soft Chemical Synthesis, Luminescent Properties, and Biomedical Applications, Chem. Rev. 114 (2014) 2343-2389.
15. X. Sun, B. Dong, H. Xu, S. Xu, X. Zhang, Y. Lin, L. Xu, X. Bai, S. Zhang, and H. Song, Amphiphilic Silane Modified Multifunctional Nanoparticles for Magnetically Targeted Photodynamic Therapy, ACS Appl. Mater. Interface 9, (2017) 11451-11460.

16. S. Yoo, J. Park, and Y. Nam, Single-Cell Photothermal Neuromodulation for Functional Mapping of Neural Networks, ACS Nano 13 (2019) 544-551.
17. G. Topcu, T. Guner, E. Inci, and M. M. Demir, Colorimetric and plasmonic pressure sensors based on polyacrylamide/Au nanoparticles, Sens. Actuators A: Phys. 295 (2019) 503-511.
18. Z. Li, C. Liao, Y. Wang, L. Xu, D. Wang, X. Dong, S. Liu, Q. Wang, K. Yang, J. Zhou, Highly-sensitive gas pressure sensor using twin-core fiber based in-line Mach-Zehnder interferometer, Opt. Express 23 (2015) 6673–6678.
19. Z. Tian, S. Yam, H. Loock, Refractive index sensor based on an abrupt taper Michelson interferometer in a single-mode fiber, Opt. Lett. 33 (2008) 1105–1107.